

Eur. Phys. J. Plus (2015) **130**: 175

DOI 10.1140/epjp/i2015-15175-4

Acoustic investigation of the aperture dynamics of an elastic membrane closing an overpressurized cylindrical cavity

Claudia Sánchez, Valérie Vidal and Francisco Melo



Società
Italiana
di Fisica



Springer

Acoustic investigation of the aperture dynamics of an elastic membrane closing an overpressurized cylindrical cavity

Claudia Sánchez¹, Valérie Vidal^{2,a}, and Francisco Melo¹

¹ Laboratorio de Física No Lineal, Departamento de Física, Universidad de Santiago de Chile, Avenida Ecuador 3493, Santiago, Chile

² Laboratoire de Physique, Université de Lyon, Ecole Normale Supérieure de Lyon - CNRS, 46 Allée d'Italie, 69364 Lyon cedex 07, France

Received: 21 April 2015 / Revised: 30 July 2015

Published online: 28 August 2015 – © Società Italiana di Fisica / Springer-Verlag 2015

Abstract. We report an experimental study of the acoustic signal produced by the rupture of an elastic membrane that initially closes a cylindrical overpressurized cavity. This configuration has been recently used as an experimental model system for the investigation of the acoustic emission from the bursting of elongated gas bubbles rising in a conduit. Here, we investigate the effect of the membrane rupture dynamics on the acoustic signal produced by the pressure release by changing the initial tension of the membrane. The initial overpressure in the cavity is fixed at a value such that the system remains in the linear acoustic regime. For large initial membrane deformation, the rupture time τ_{rup} is small compared to the wave propagation time in the cavity and the pressure wave inside the conduit can be fully captured by the linear theory. For low membrane tension, a hole is pierced in the membrane but its rupture does not occur. For intermediate deformation, finally, the rupture progresses in two steps: first the membrane opens slowly; then, after reaching a critical size, the rupture accelerates. A transversal wave is excited along the membrane surface. The characteristic signature of each opening dynamics on the acoustic emission is described.

1 Introduction

Releasing pressure from an initially closed cavity can produce different types of sound, the most famous being the “pop” sound which is heard when opening a bottle of wine or champagne. After pouring the champagne in a glass, a subtle sound can still be heard, from the bubbles bursting at the liquid free surface. In this last case, the bubbles themselves play the role of small overpressurized cavities, suddenly opening at the liquid surface. Different mechanisms can explain the generation of an acoustic wave by an overpressure release. If the geometry consists of a large volume closed by a short neck, the system can be described as a Helmholtz resonator. The acoustic wavelength is then much larger than the system dimensions. Bubbles bursting at the free surface of water, for instance, act as Helmholtz resonators [1, 2]. If the shape is round, and the cavity is open by an instantaneous removal of the cap (*e.g.* immediate removal of a round bubble film), the problem is analogous to a bursting balloon and a N-shaped wave is generated [3, 4]. Finally, if the shape is elongated, such as a bubble rising and bursting in a conduit [5] or at the surface of a non-Newtonian fluid [6, 7], or an overpressurized tube, the opening of one end of the system will give rise to longitudinal, resonant acoustic modes [8–10].

This last geometry is interesting for many applications. In particular, it has been used to model the bursting of giant, overpressurized gas bubbles (“slugs”) at the top of volcanic conduits [11, 12]. This topic is a challenge in volcanology. Indeed, retrieving information from the acoustic emissions on volcanoes could provide important clues on the volcano explosivity [13, 14]. However, the link between the acoustic waveform characteristics and the slug properties (geometry, overpressure, bursting dynamics) is yet to be assessed.

In this framework, previous studies have used liquid films closing a rigid, cylindrical cavity to model such systems—the cavity here being analogous to the bubble body, which remains almost still during the whole duration of the acoustic signal emission at bursting [9, 11]. The film is stretched over the open end of the cavity, then gas is injected

^a e-mail: valerie.vidal@ens-lyon.fr

until reaching an overpressure ΔP . The system is then let to evolve: the liquid film, which is bulged, drains under the effect of gravity, then bursts spontaneously. The acoustic signal emitted at bursting has been studied both inside and outside the cavity, which makes it possible to quantify the energy balance. In this experimental configuration, all the parameters are controlled: geometry, overpressure, etc. The acoustic signal is well described by a linear theory of longitudinal, resonant modes in the cavity: the fundamental frequency is imposed by the cavity geometry, and the damping is mainly due to radiation and viscous dissipation processes [9]. These studies pointed out the drastic effect of the film rupture time, τ_{rup} , on the acoustic signal amplitude, a parameter which could not be controlled in this setup. In particular, it has been shown that when the film rupture time becomes comparable or larger than the typical wave propagation time in the cavity, $\tau_{\text{prop}} = 2L/c$, where L is the cavity length and c the sound speed, the acoustic amplitude drastically decreases [11]. Another work considering bubble bursting at the surface of a viscous fluid in a cylindrical conduit also pointed out the direct correlation between the film rupture dynamics and the amplitude of the acoustic wave produced at bursting [8]. However, considering bubble bursting in fluids or closing a cavity with liquid films does not allow to model high overpressures, whereas on volcanoes, for instance, bubble overpressures can be of the order of a few kPa and up to several MPa [15–20].

In a recent work, the acoustic signal produced by the overpressure release of a cavity initially closed by an elastic membrane has been reported [12]. In this configuration, it is possible to reach overpressures up to 50 kPa, and the transition toward nonlinear acoustic regimes has been studied. However, all the experiments were performed with membranes initially stretched well enough to ensure the rupture time would be small (of the order of 0.2 ms) and not affect the acoustic amplitude.

In the present study, we investigate experimentally the role of the membrane rupture time on the acoustic signal emitted during the overpressure release of a cylindrical cavity. The membrane opening time is controlled by tuning its initial stretching over the open end of the cavity. Note that we consider the emission of an acoustic wave, so we always have in our experiments a membrane rupture time, τ_{rup} , smaller than the wave propagation time in the cavity, τ_{prop} . The work is limited to linear acoustic regimes, *i.e.* initial overpressure in the cavity well below the transition threshold to nonlinear effect, $\Delta P_c \simeq 24$ kPa [12]. We aim at characterizing the membrane rupture dynamics and its connection with the acoustic emission both inside and outside the cavity. In particular, for a slow opening we point out the existence of a transversal wave propagating on the membrane, which gives rise to an additional wave in the acoustic signal.

2 Experimental setup

The experimental device (fig. 1(a)) consists of a cylindrical cavity (length $L = 0.60$ or 0.32 m, inner diameter $\Phi = 25.4$ mm) drilled in plexiglas. The tube is hermetically sealed at the bottom end (rigid bottom) and an elastic membrane (latex, thickness $e = 0.5$ mm) stretched manually and fixed by a mechanical device closes the upper end of the tube. Air is then injected in the cavity through an inlet of 3 mm diameter located at 2 cm from the tube bottom, up to a controlled overpressure ΔP . In this experiment, we impose an initial overpressure $\Delta P \simeq 5$ kPa, in order to be in the linear acoustic regime [12]. A circle initially printed on the membrane at rest (radius R_0) makes it possible to quantify the membrane deformation ε , given by $\varepsilon = (R - R_0)/R_0$, after stretching and imposing the overpressure in the cavity (fig. 1(b)). Note that the first membrane deformation, ε_i due to stretching only, is imposed in the absence of overpressure, *i.e.* for the flat membrane. Increasing the overpressure increases the strain by imposing a curvature. However, the curvature is small for the overpressure used in this experiment ($\Delta P \simeq 5$ kPa), and the difference can be neglected, $\varepsilon \simeq \varepsilon_i$. In our experiment, we explore the range $0.3 < \varepsilon < 3$.

At time $t = 0$ a needle of typical diameter 0.1 mm, fixed on a motorized arm, pierces the center of the elastic membrane, which ruptures suddenly. A Phantom v9.1 high-speed video camera is used to record the membrane rupture dynamics at typical rates from 16000 to 24000 frames per second (fps). The membrane is illuminated from above and from the side to record both the rupture and wave propagation on the membrane (see sect. 3.3). The rupture time, τ_{rup} , is defined as the time taken by the fracture tip to reach the tube boundary (fig. 1(c)).

The acoustic wave produced by the overpressure release is monitored at the bottom of the cavity (force sensor PCB 200B02 + amplifier PCB 482A16, PCB Piezotronics). We chose to focus on the signal inside rather than outside the cavity, to avoid waveform change and additional energy loss due to the radiation pattern outside. The signal is recorded by means of an oscilloscope (Tektronix TDS2012B, sampling frequency 25 kHz).

3 Experimental results

Different rupture dynamics of the elastic membrane are observed, depending on the membrane initial deformation (fig. 1(d)). For large initial strain (i), the fracture propagates immediately after piercing; for intermediate strain (ii), a crack opens slowly, until the fracture length reaches a critical value, l_c , at which the fracture suddenly accelerates

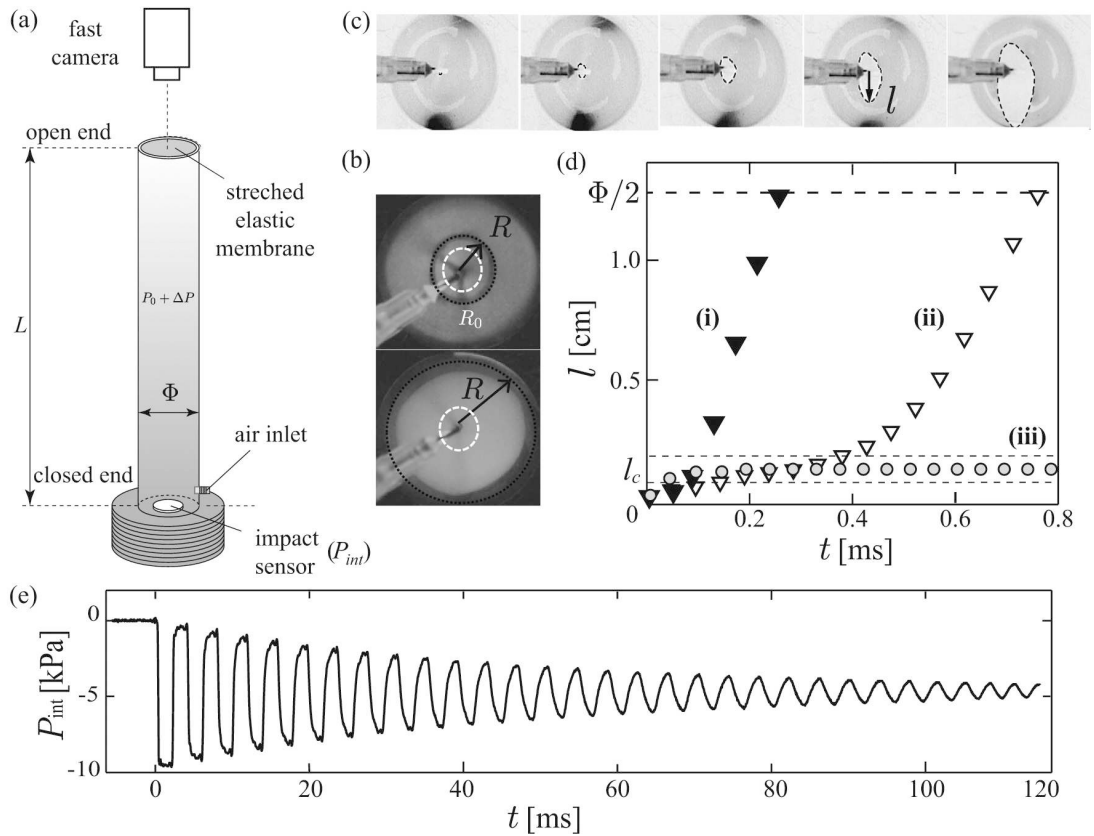


Fig. 1. (a) Experimental setup. We impose an overpressure ΔP by injecting air inside a cylindrical cavity (length L) closed by an elastic membrane. When the membrane bursts, the acoustic signal, P_{int} , is recorded at the bottom of the cavity. The high-speed camera records the rupture of the elastic membrane from above the tube. (b) Measurement of the membrane deformation ε before bursting. The white dashed circle indicates the printed mark on the membrane at rest; the black dotted circle is the mark on the deformed membrane, under pressure (radius R). Top: small membrane deformation [$\varepsilon = 0.7$]. Bottom: large membrane deformation [$\varepsilon = 3$]. (c) Image sequence of the membrane rupture [$\Delta t = 12.6 \times 10^{-5}$ s between each image]. The rupture time, τ_{rup} , is taken as the time for the fracture (length l) to reach the tube boundary. (d) Crack length l as a function of time, for different initial strain [$L = 32$ cm; (i) $\varepsilon \sim 2.8$, (ii) $\varepsilon \sim 1.3$, (iii) $\varepsilon \sim 0.5$]. The horizontal dashed lines indicate the range of critical length l_c above which a crack can propagate on the membrane (see fig. 4(b)). (e) Amplitude of the acoustic wave at the bottom of the tube, as a function of time [$L = 32$ cm, $\varepsilon \sim 2.8$, $\tau_{\text{rup}} \sim 0.2$ ms]. The waveform is nearly squared at early stages due to multiple rebounds of the acoustic front.

until reaching the cavity boundary; for sufficiently low strain (iii), the fracture grows slowly then stops, leading to the formation of a small and stable hole in the membrane center.

Figure 1(e) displays a typical pressure signal inside the cavity, as detected by the sensor at the bottom, for a fast membrane opening (regime (i)). At early stages the wave is nearly squared, as the pressure front generated by the membrane rupture travels back and forth in the cavity. Indeed, it is reflected both at the cavity bottom (rigid boundary condition) and at the open end (acoustic impedance mismatch). The acoustic signal is then damped in time, and becomes more sinusoidal (see sect. 3.2.1). Note that due to the reflection conditions, the acoustic amplitude at the cavity bottom should first drop from $+\Delta P$ to $-\Delta P$. As the force sensor inside the cavity is not able to measure DC component, the pressure wave drops from 0 to $-\Delta P$, then oscillates towards $-\Delta P$ instead of the expected zero. If we wait for a much longer time, the sensor indeed relaxes to zero. As its relaxation time is much larger than the typical duration of the acoustic signal, the only consequence in our measurements is a systematic shift of $-\Delta P$ for the signal inside the cavity (P_{int}), which we did not correct here in order to display the raw signals. In the following, we thoroughly describe the characteristics of the acoustic waveform, and the link between the membrane rupture dynamics and the acoustic emission.

3.1 Control of the rupture time

We first investigate the dependence of the membrane rupture time, τ_{rup} , as a function of its initial stretching before bursting, ε (fig. 2(a)). As expected, τ_{rup} is a decreasing function of ε and does not depend on the tube length, L .

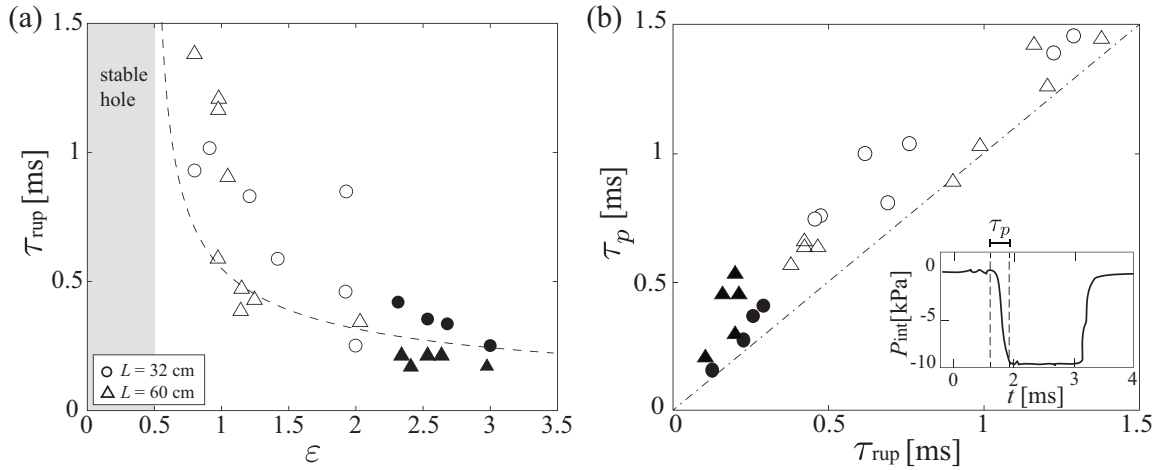


Fig. 2. (a) Membrane rupture time, τ_{rup} , as a function of the membrane strain, ε . The dashed line represents the fit for the fast opening regime ($\varepsilon \geq 2$), $\tau_{rup} = a/\sqrt{\varepsilon}$, with $a = 0.4$ ms, when shifting the origin at $\varepsilon_0 = 0.5$, *i.e.* excluding the region where the membrane does not open (see text) ((symbol, L): (o, 32 cm), (Δ , 60 cm)). The colors indicate the different opening regimes: (i) black symbols, fast opening [$\varepsilon \sim 2.2$ –3]; (ii) white symbols, two-step opening [$\varepsilon \sim 0.5$ –2]; (iii) gray zone, stable hole [$\varepsilon < 0.5$]. (b) Pressure drop characteristic time, τ_p , *vs.* rupture time τ_{rup} (same legend as (a)). The dashed line indicates the slope 1 line. Inset: Measurement of the pressure drop characteristic time, τ_p [$L = 32$ cm, $\varepsilon \sim 3$].

Note that we always check the condition for sound generation, $\tau_{rup} < \tau_{prop}$ [9, 11]. Indeed, by taking $c = 346$ m s⁻¹ as the sound speed at 25 °C, we have $\tau_{prop} \simeq 1.8$ ms and $\tau_{prop} \simeq 3.5$ ms for $L = 0.32$ and 0.60 m, respectively. The experimental data can be fitted by $\tau_{rup} \sim \varepsilon^{-1/2}$, when shifting the origin at $\varepsilon_0 = 0.5$, the threshold above which the membrane ruptures (see sect. 3.2.3). The dependence of τ_{rup} on ε can be explained by considering the fracture speed dependence on the membrane initial strain (see sect. 3.4). Note that an experimental point stands clearly out of the main tendency (white point at $\varepsilon \sim 2$). In that case, we observe the material softening, as τ_{rup} unusually increases. This outlier can be explained by the Mullins' effect, which states that rubber-like materials exhibit a change in their mechanical properties when stretched, and hysteresis under cycling loading [21–23]. In all our experiments, the latex membrane is usually stretched only once. As the rupture time is measured directly by the high-speed camera, we will not consider further the experiments which present such peculiar behavior.

Although previous studies quantified the correlation between the amplitude of the acoustic signal produced when a bubble bursts at the surface of a viscous fluid by direct measurements of the film aperture dynamics [8], it is not always possible to access the fast film dynamics. In a previous work investigating the bursting of a liquid film initially closing an overpressurized cavity, and the associated acoustic signal, the authors proposed an estimation of the rupture time as the first pressure drop characteristic time at the bottom of the cavity [9]. However, the direct relationship between these two variables was not quantified. In our experiment, the simultaneous acquisition of the high-speed images of membrane rupture and the acoustic signal inside the cavity makes it possible to check this correlation (fig. 2(b)). We confirm the direct relationship between the first pressure drop characteristic time, τ_p , and the membrane rupture time, τ_{rup} . In most experiments, we note that $\tau_p \geq \tau_{rup}$. A possible explanation is that the surface of the opening continues increasing even for $t > \tau_{rup}$, due to the fact that the crack on the membrane is anisotropic (see fig. 1(c)). The surface area of the opening changes the waveform, and may be at the origin of this systematic trend. In the following, we describe the acoustic waveform generated by the overpressure release, for the different opening dynamics.

3.2 Different opening dynamics

3.2.1 Fast membrane opening

We first investigate the acoustic waveform inside the cavity after bursting in the fast rupture regime (regime (i), fig. 1(d)), *i.e.* when the membrane initial strain is high ($\varepsilon \sim 2$ –3). Figure 3 displays the pressure signal inside the cavity and its respective power spectrum for two different membrane rupture times, both in the fast opening regime. As already described in previous experiments [9, 12], the overpressure release generates longitudinal resonant acoustic modes in the cavity. Due to the asymmetric boundary conditions (rigid bottom end and open top end), only odd harmonics are excited. The pressure signal inside the cavity displays a square waveform, as it contains all the odd harmonics (low and high frequencies), and the acoustic front rebounds back and forth in the cavity [9]. The cavity length directly governs the frequency content, and the acoustic energy informs about the characteristic time associated

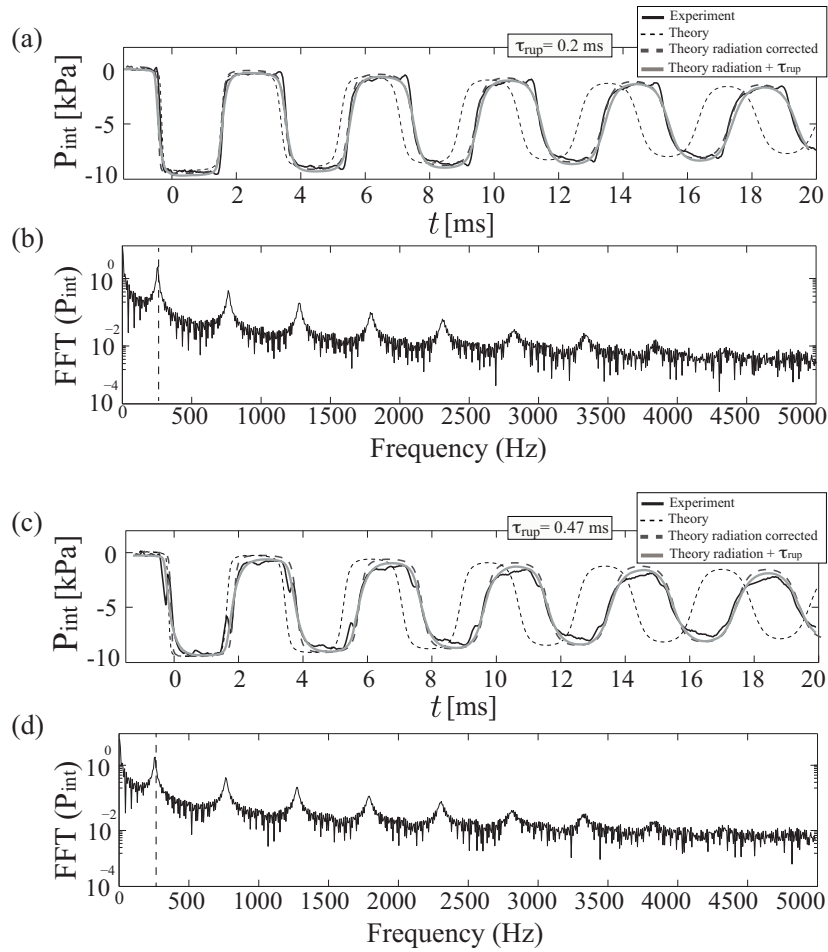


Fig. 3. Pressure signal inside the cavity, P_{int} (black line), zoomed on the first 20 ms, and total signal spectrum for different rupture time ((a,b) $\tau_{\text{rup}} = 0.23$ ms, $\varepsilon = 2.8$. (c,d) $\tau_{\text{rup}} = 0.47$ ms, $\varepsilon = 2$; $L = 32$ cm). The theoretical prediction is represented in the upper panels (a) and (c), when taking into account different terms: model without rupture time and no radiation correction, $\nu_0 = c/4L$ (dotted line), model without rupture time and with radiation correction, $\nu'_0 = c/4L'$ (dashed line), model with rupture time and radiation correction (gray line). The dashed vertical line in the spectrum (b) and (d) indicates the theoretical frequency of the fundamental mode, when considering the radiation correction.

with the cavity opening, more than about the energy initially loaded in the cavity [9]. Moreover, the radiation of the acoustic wave outside the cavity and viscous dissipation along the walls are responsible for the signal damping over time. Note that the higher harmonics are damped faster, so the square acoustic waveform inside the cavity becomes more sinusoidal in time, until only the fundamental mode remains [9].

In order to describe the signal shape and its frequency content, we remind previous theoretical results modeling the acoustic pressure inside the cavity, P_{int} , in the linear regime, when the overpressure is released over a characteristic time τ_p [9]. It is given by

$$\frac{P_{\text{int}}(t)}{\Delta P} = e^{-t/\tau_p} + \sum_{n=0}^{\infty} a_n \sin[\omega_n t + \theta_n] e^{-t/\tau_n^d}, \quad (1)$$

where the frequency ω_n , amplitude a_n and phase θ_n of the mode n are defined by

$$\omega_n \equiv (2n + 1) \frac{\pi c}{2L} \quad (2)$$

$$a_n \equiv \frac{4 \omega_0}{\pi \omega_n} \frac{(-1)^n}{\sqrt{1 + (\omega_n \tau_p)^2}} \quad (3)$$

$$\tan(\theta_n) \equiv \frac{1}{\omega_n \tau_p}, \quad \theta_n \in \left[0, \frac{\pi}{2}\right]. \quad (4)$$

$c \simeq 346 \text{ ms}^{-1}$ is the sound speed at room temperature, $T \simeq 298 \text{ K}$, and τ_n^d denotes the characteristic damping time for mode n ,

$$\frac{1}{\tau_n^d} = \frac{1}{\tau_n^Z} + \frac{1}{\tau_n^{r_0}} + \frac{1}{\tau_n^v}, \quad (5)$$

which accounts for the characteristic damping time due to radiation outside the cavity, τ_n^Z , reflection at the cavity bottom, $\tau_n^{r_0}$, and viscous dissipation at the cavity walls, τ_n^v . These characteristic dissipation times can be written as

$$\tau_n^Z = \frac{1}{2\pi^2} \left(\frac{c}{\Phi} \right)^2 \left(\frac{2n+1}{\nu_n^3} \right), \quad (6)$$

$$\tau_n^{r_0} = \left(\frac{1-r_0}{1+r_0} \right) \frac{1}{4\nu_n}, \quad (7)$$

$$\tau_n^v = \frac{\Phi}{2\sqrt{\pi\eta[1+(\gamma-1)P_r^{-1/2}]}} \left(\frac{1}{\nu^{1/2}} \right), \quad (8)$$

where $\nu_n = \omega_n/2\pi$. r_0 is the reflection coefficient at the cavity bottom, $\eta = 1.5 \times 10^{-5} \text{ m}^2 \text{ s}^{-1}$ the air kinematic viscosity, $P_r \simeq 0.7$ the Prandtl number, and $\gamma = 1.4$ the specific heat ratio. As already pointed out in a previous work [9], the dissipation time, whichever the mechanism, decreases when the frequency increases, meaning that higher harmonics are dissipated faster than the fundamental, and dissipation is larger for smaller tubes.

The only adjustable parameter in the model is the reflection coefficient at the bottom end of the cavity, r_0 . It is taken as $r_0 = -0.97$, in order to best fit the damping of the acoustic signal. Figure 3(a) displays the measured acoustic signal (black line), for an initial membrane strain $\varepsilon \sim 2.8$ (observed rupture time $\tau_{\text{rup}} \sim 0.2 \text{ ms}$). The signal computed from the model (eq. (1)) is also displayed, when taking into account the different terms. First, we represent the waveform without taking into account the rupture time, and using the theoretical tube frequencies given by $\nu_n = (2n+1)\nu_0$, where $\nu_0 = c/4L = 270 \text{ Hz}$ is the fundamental frequency (dotted line, fig. 3(a)). A systematic phase shift with the experimental data is observed, indicating that frequency correction due to the radiation of the acoustic wave outside the cavity must be introduced [24–27]. Indeed, the experimental power spectrum (fig. 3(b)) indicates that the vibration frequencies differ slightly from those given by the tube length only, but they obey to the same progression and display the odd harmonics only, $\nu'_n = (2n+1)\nu'_0$, due to asymmetric boundary conditions of the cavity. To the first order in Φ/L , the wave radiation outside the cavity introduces a correction length δL , which leads to a slight increase in the wavelength

$$\lambda'_n = \frac{4}{2n+1}(L + \delta L) \quad (9)$$

and, accordingly, to a slight decrease in the frequency $\nu'_n = c/\lambda'_n$. The correction length, δL , is expected theoretically to be $\delta L = 4\Phi/3\pi$ for a flanged aperture (half-space radiation) [25–27], and $\delta L = 0.3\Phi$ for an unflanged aperture (full space radiation) [24, 25]. The experimental frequencies, measured from the signal spectrum (fig. 3(b)), give an effective tube length $L' = L + 0.9\Phi$, which is consistent with the order of magnitude of the theoretical correction. Introducing this correction in the model shows a satisfactory agreement with the experimental waveform (dashed line, fig. 3(a)).

Finally, although the rupture time is short in this fast opening regime (i), we can take it into account in the model (eq. (1)). The rupture time in the model, τ_p , corresponds to the characteristic time of the first pressure drop, as displayed in fig. 2(b), inset, and is directly correlated to the membrane rupture time, as measured from fig. 1(c) (see fig. 2(b)). The additional correction is small (gray line, fig. 3(a)), but visible when τ_{rup} is of the order of 0.4–0.5 ms (gray line, fig. 3(c)). Note that it captures well the small distortion of the signal, as it accounts for the delayed rise and drop of the pressure front for each acoustic signal period.

Thus, despite the relative high level of overpressure ($\Delta P \simeq 5 \text{ kPa}$), the linear theory accurately accounts for the acoustic waveform inside the cavity. The only adjustable parameter, τ_p , the characteristic time of the first pressure drop in the cavity, can be directly related to the membrane rupture time.

3.2.2 Opening in two steps

When the membrane is subjected to intermediate strain (ε ranging from 0.5 to 2), the rupture occurs in two steps (fig. 1(d), regime (ii)). First, the hole triggered by the needle at the membrane center grows slowly, and remains nearly circular. This slow propagation is followed by a sudden increase of the aperture velocity of the membrane, which resembles more a crack propagation.

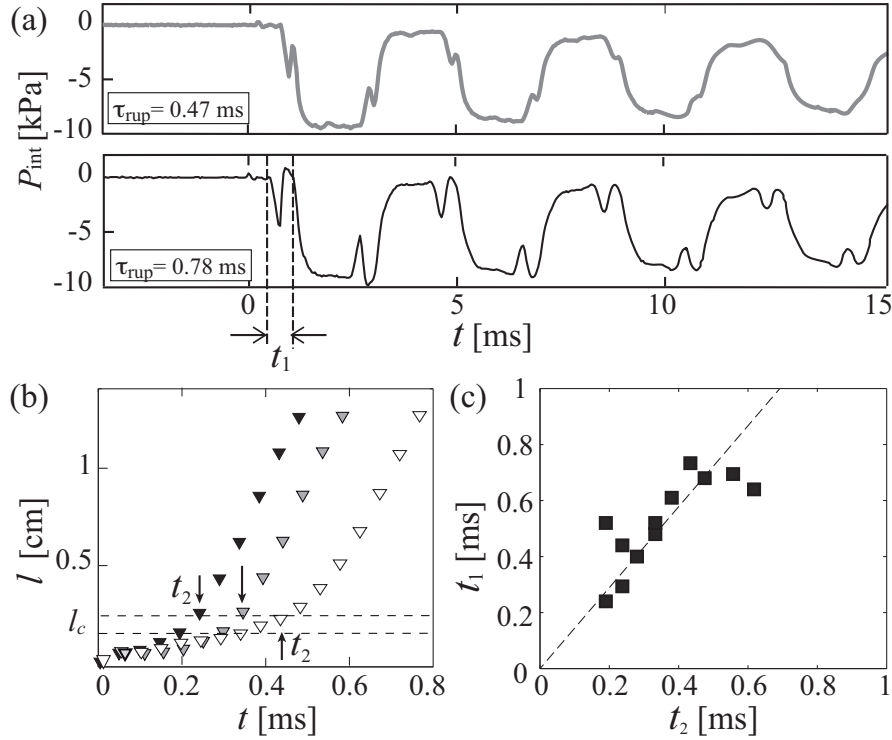


Fig. 4. (a) Pressure signal inside the tube (P_{int}) for two intermediate rupture time, zoomed on the first 15 ms. Up: $\varepsilon \sim 2$, $\tau_{\text{rup}} \sim 0.47$ ms. Down: $\varepsilon \sim 1.2$, $\tau_{\text{rup}} \sim 0.78$ ms [$L = 32$ cm]. (b) Crack length as a function of time, for different membrane initial deformation ((color, ε): (black, 2); (gray, 1.5); (white, 1)). The black arrows indicate the cross-over time, t_2 , and the dashed lines indicate the range of l_c (see text). (c) Time delay t_1 vs. cross-over time t_2 . The dashed line indicates the linear fit, $t_1 = 1.4t_2$.

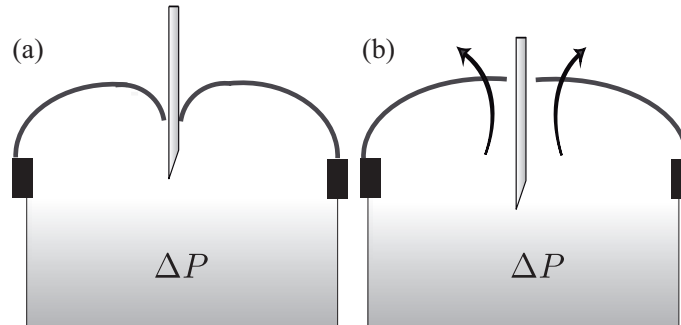


Fig. 5. Sketch of the membrane piercing (view from the side). (a) Due to the needle indentation, the membrane develops a cusp at the center. (b) The elastic response of the membrane, right after piercing, generates an upward motion, hence a small pressure drop in the cavity.

In this regime, we observe an additional wave in the acoustic signal, which amplitude increases when the rupture time increases (fig. 4(a)). Immediately after piercing, the inside pressure depicts a small oscillation, followed by a sudden pressure decrease, whose time delay is indicated by t_1 (fig. 4(a), lower panel). The main pressure drop (equal to $2\Delta P$) is the usual overpressure released, already observed for the fast membrane opening regime (sect. 3.2.1).

We interpret the first oscillation, mainly characterized by a negative peak, as the elastic relaxation of the membrane after piercing by the needle. When the needle tip is pushed on the top of the membrane, before bursting, it often develops a cusp, due to the elastic response of the membrane (fig. 5(a)). Right after piercing, due to both the elastic response and the overpressure release through the hole, the membrane edge close to the needle exhibits an upward motion (fig. 5(b)), and hence generates a small pressure drop in the cavity. This motion is at the origin of the additional wave in the acoustic signal (fig. 4(a)). Together with the main pressure drop, this disturbance is reflected at the top and bottom of the cavity, and has therefore the same periodicity, $4L/c$. Note that except for this additional disturbance, the acoustic signal has the same characteristics than for a fast opening membrane (see sect. 3.2.1): the fundamental frequency is given by the cavity length, $\nu_0 = c/4L$, and only the odd harmonics appear in the spectrum, due to the asymmetric boundary conditions of the cavity.

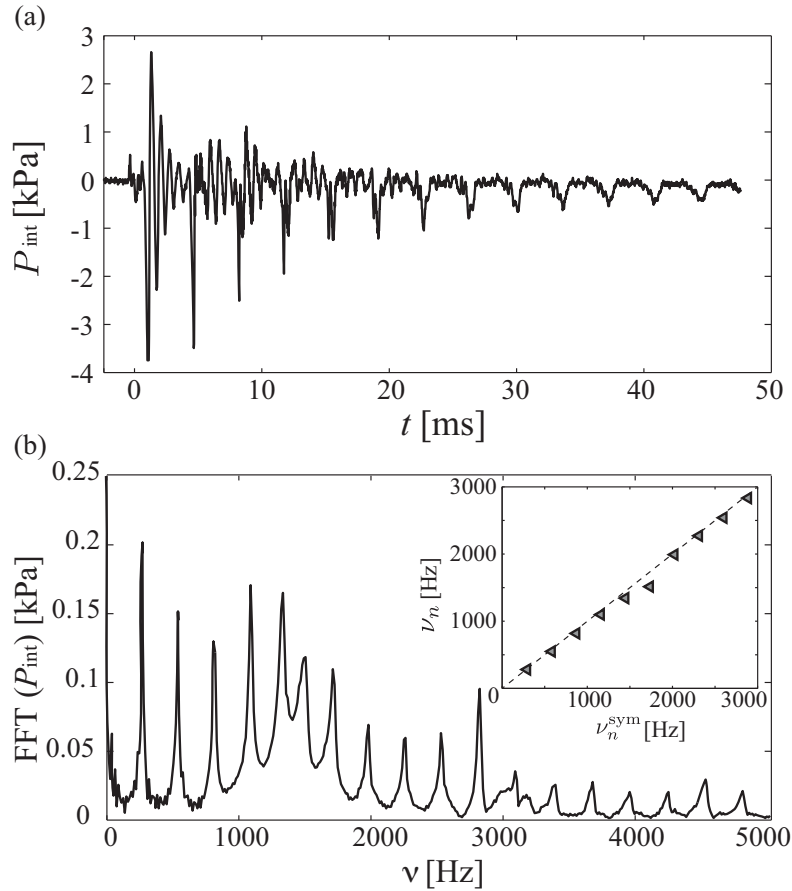


Fig. 6. (a) Pressure signal at the bottom of the cavity, P_{int} , as a function of time when the crack does not propagate on the membrane (stable hole) ($L = 60$ cm, $\varepsilon = 0.5$). (b) Power spectrum of the signal displayed in (a). Inset: Harmonic frequency of mode n , ν_n (power peak in the spectrum, experimental data) vs. theoretical harmonics ν_n^{sym} computed for a tube $L = 60$ cm with symmetric boundary conditions (both ends closed, see text). The dashed line indicates a linear relationship (slope 1).

Figure 4(b) displays the temporal evolution of the crack length, l , for different initial strain ε . The cross-over between the two opening steps is characterized by a critical size of the fracture, l_c , which is reached in a time t_2 (dashed line and black arrows, fig. 4(b)). To check the correlation between the opening dynamics and the additional acoustic wave, we plot the time delay t_1 , measured directly on the acoustic signal (fig. 4(a)), as a function of the cross-over time, t_2 (fig. 4(c)). The linear relationship between these two quantities indicates that this additional waveform is directly linked to the opening dynamics of the membrane.

3.2.3 Stable hole

For low initial membrane deformation ($\varepsilon < 0.5$), the membrane does not rupture completely. After piercing by the needle, a small hole grows slowly, up to a radius of about 2 mm, after which the opening stops, and the hole remains stable (fig. 1(d), regime (iii)). The pressure release induced by this process also triggers an acoustic wave inside the cavity (fig. 6(a)), but with different characteristics than the one described above (sects. 3.2.1 and 3.2.2). First, the acoustic signal does not display the same oscillatory waveform than for a full opening (see fig. 1(e), for example). Then, its harmonic content (fig. 6(b)) is different than the resonance of the cavity with asymmetric boundary conditions—compare, for example, to the spectrum displayed in fig. 3(b).

Although the overpressure release is enough to excite an acoustic wave in the cavity, as the hole remains small respect to the tube diameter Φ , the cavity behaves as a resonator with symmetric boundary conditions, with closed ends both at its top and bottom. Figure 6(b), inset, compares the measured signal frequencies to the theoretical frequencies of the harmonics developing in a cavity closed at both ends, $\nu_n^{\text{sym}} = (n + 1)\nu_0^{\text{sym}}$ with $\nu_0^{\text{sym}} = c/2L = 280$ Hz. The dashed line indicates that the resonance is indeed that of a closed cavity. Note that in spite of the typical geometry resembling a cavity with a short neck, we do not find here any signature of a Helmholtz resonance. Indeed, the Helmholtz frequency is given by $f_H = (cr/2)\sqrt{1/\pi eV}$ where r is the aperture radius, e the membrane thickness (aperture length), and $V = \pi(\phi^2/4)L$ the cavity volume. For a tube length $L = 0.32$ cm, and $r \simeq 2$ mm, $f_H \simeq 685$ Hz,

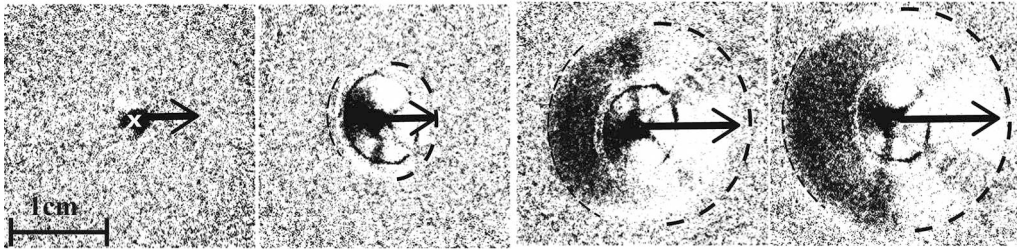


Fig. 7. Surface wave propagating on the membrane right after piercing. The images are obtained by successive image difference with the high-speed video camera. This wave is radial, and rebounds on the tube boundaries are often observed. The black arrow indicates the propagation of the wave front (dashed circle) in one direction, for wave velocity computation ($L = 32$ cm, $\Delta t = 4.5 \times 10^{-5}$ s between each image, $\varepsilon = 0.5$, $v_w = 29$ m s $^{-1}$).

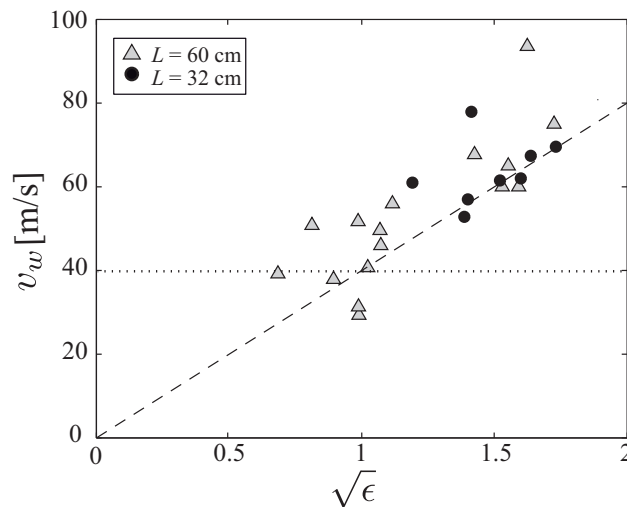


Fig. 8. Velocity of the wave propagating on the membrane surface, as a function of the square root of the strain ε . The horizontal dotted line corresponds to the theoretical velocity of a longitudinal wave. The dashed line is the prediction for the wave velocity assuming a transversal wave, without any adjustable parameters (see text).

which has no signature on the acoustic signal spectrum (fig. 6(b)). If we consider that the membrane gets thinner due to the stretching, the Helmholtz frequency is even higher.

As the rupture is not fully completed in this regime, it will not be considered further. In the following, we will focus on the intermediate regime (ii), and on the membrane dynamics.

3.3 Wave along the membrane

The membrane elastic response, at the origin of the additional wave on the acoustic signal, generates a wave which propagates radially on the membrane surface, and which can be clearly observed in the low or intermediate strain regime ($\varepsilon \lesssim 2$, fig. 7). If the membrane opens slowly, the wave travels faster than the rupture growth, and rebounds on the tube boundary. The rebounds are also observed in regime (iii), when the hole remains stable. The wave front can be detected by registering the intensity variations of the light reflected by the membrane. Contrast is improved by considering successive images difference, in order to extract the wave front and, thus, the wave velocity, v_w . Typically, $v_w \simeq 40$ m s $^{-1}$ for a strain $\varepsilon \simeq 0.7$.

In order to identify the nature of the wave propagating along the membrane, we investigate the velocity dependence on membrane tension. The experimental data are reported in fig. 8. Although scattered, they show a roughly linear dependence of the wave speed on the square root of the membrane strain, $v_w \sim \sqrt{\varepsilon}$. As expected, this scaling is independent of the cavity length, L .

Previous works have investigated the characteristics of longitudinal waves excited by rubber band recoil [28]. The authors have shown that the wave speed, v_l , is independent of the initial membrane tension and can be written $v_l = \sqrt{E/\rho}$, where E is the Young modulus and ρ the density of the latex membrane. By considering the properties of the membrane used in our experiments, $E \simeq 1.5 \times 10^6$ Pa and $\rho \simeq 920$ kg m $^{-3}$, we get $v_l \simeq 40$ m s $^{-1}$. Although this value is of the order of magnitude of the wave speed measured experimentally, it does not capture the dependence on $\sqrt{\varepsilon}$, as the longitudinal wave velocity is independent of the initial strain ε (dotted line, fig. 8).

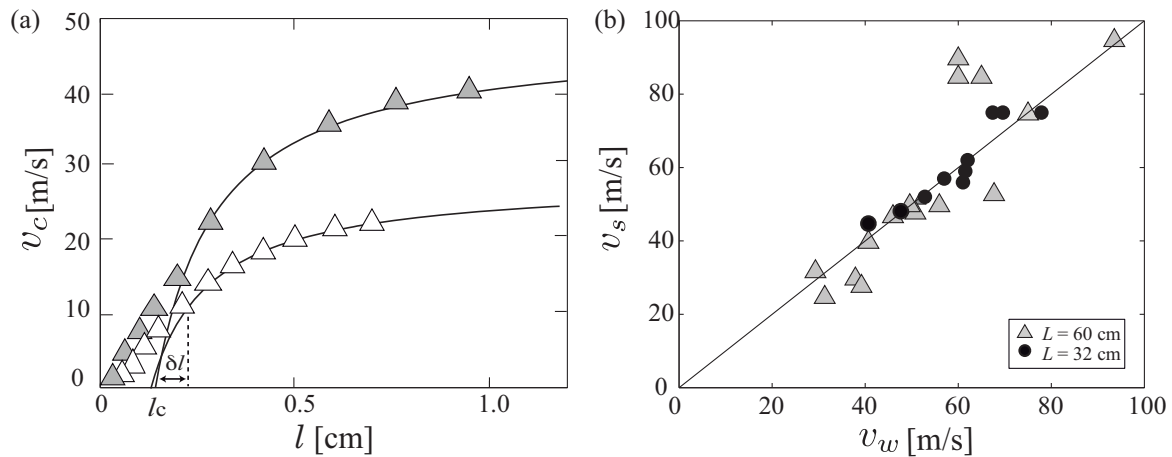


Fig. 9. (a) Crack velocity v_c as function of the crack length l for different initial strain ((color, ε): (white, 1); (gray, 2)). The black line is the fit with the theoretical prediction for fracture propagation (eq. (11)) with the adjustable parameters (v_s, l_c) ($L = 60$ cm). ($l_c + \delta l$) indicates the length at which the crack enters the fast opening regime (see text). (b) Characteristic wave velocity v_s obtained by adjusting the crack speed (a) with the prediction of fracture propagation, plotted against the measured speed of transverse waves v_w , for different tube length and different initial strain ($0.5 \lesssim \varepsilon \lesssim 3$). The black line indicates the slope 1 line.

Conversely, the velocity of a transverse elastic wave is a function of the membrane tension σ , and writes

$$v_t = \sqrt{\frac{\sigma}{\rho}} \approx \sqrt{\frac{\varepsilon E}{\rho}}. \quad (10)$$

The dashed line in fig. 8 shows the theoretical prediction for the transversal wave velocity, without any adjustable parameters. The theory nicely captures the experimental data trend. We therefore conclude that, in our system, the wave observed on the membrane is a transverse wave, excited by the curvature change when initially piercing with the needle (fig. 5). This transversal wave is mainly responsible for the partial stress relaxation taking place immediately after piercing. It is at the origin of the additional wave observed in the acoustic signal.

3.4 Link with fracture dynamics

In the following we investigate the membrane rupture process in more detail. If considering the crack growth on the membrane in the framework of fracture propagation in a brittle material, the crack speed, v_c , is given by [29]

$$v_c = v_s \left(1 - \frac{l_c}{l}\right), \quad (11)$$

where l_c is the minimum fracture length above which the crack can propagate, l is the total crack length and v_s the characteristic wave velocity on the membrane. Using best fits of the experimental data of the crack propagation velocity, v_c , as a function of the crack length, l (fig. 9(a)) and eq. (11), we extract the characteristic wave velocity v_s and the critical crack length l_c for different experimental parameters.

Figure 9(b) shows good agreement between v_s and the direct measurement of the transversal wave velocity on the membrane. The critical length obtained from the fit ranges from $l_c = 1.5$ to 2.5 mm. This result is consistent with the value found for the cross-over length at which the crack suddenly accelerates, in the two-step opening regime (ii) (fig. 4(b)). Strictly, in the brittle fracture framework, l_c is the length for which the stress concentration at the crack tip is sufficient to allow for crack propagation. Thus, l_c is expected to decrease with external stress (or equivalently ε) and increase with the size of the crack tip, although it could not be checked in our experiments due to data dispersion. In our experiment, the size of the crack tip is likely fixed by the size of the sharp end of the needle, at least at crack initiation. For large ε , the length of the initial crack easily exceeds $l_c(\varepsilon)$. For intermediate ε , the initial crack size is smaller than $l_c(\varepsilon)$, so a brittle crack does not propagate immediately. A slower process of crack opening is first observed, which is more likely a plastic deformation taking place at the crack tip. For small ε , the tension is too small and even the crack progression through a relaxation process cannot occur.

As the results above point out that the membrane rupture can be described in the framework of brittle failure, the theoretical predictions can account for the rupture time dependence as a function of strain (fig. 2(a)). Indeed, in the regime where the fracture strongly accelerates ($l \geq l_c + \delta l$), we can write

$$\tau_{\text{rup}} = \int_{l_c + \delta l}^{\frac{\Phi}{2}} \frac{dl}{v_c} \simeq \frac{\sqrt{\rho/E}}{\sqrt{\varepsilon}} \int_{l_c + \delta l}^{\frac{\Phi}{2}} \frac{dl}{(1 - l_c/l)}, \quad (12)$$

by using eq. (11), $v_s \simeq v_w$ (fig. 9) and $v_w = v_t = \sqrt{\varepsilon E/\rho}$ (eq. (10)). This leads to the formal expression:

$$\tau_{\text{rup}} = \sqrt{\frac{\rho}{E}} \left[\left(\frac{\Phi}{2} - l_c \right) + l_c \ln \left(\frac{\frac{\Phi}{2} - l_c}{\delta l} \right) \right] \frac{1}{\sqrt{\varepsilon}}. \quad (13)$$

We therefore have $\tau_{\text{rup}} = a/\sqrt{\varepsilon}$, in agreement with the experimental data. If we use the value of the coefficient given by the fit, $a \simeq 0.4$ (dashed line, fig. 2(a)), we find $\delta l \simeq 0.7$ mm, in agreement with the estimation from fig. 9(a), when taking into account the length after which the fracture propagates in the fast regime. In the intermediate regime, the slow propagation mode increases, which explains why the experimental data are above the trend (fig. 2(a)).

4 Discussion and conclusion

Based on the experimental study of the acoustic signal produced by the rupture of an elastic membrane that initially closes a cylindrical overpressurized cavity, we have characterized the link between the membrane rupture dynamics and the acoustic waveform inside the cavity. The results confirm previous hypothesis of the direct relationship between the characteristic opening time of the cavity and the first pressure drop on the acoustic signal, and underline once again the drastic importance of this parameter on the acoustic wave generation.

We show that the acoustic signal produced by the pressure release strongly depends on the membrane rupture dynamics. For large membrane initial deformation (strain $\varepsilon > 2$), the rupture time τ_{rup} is short compared to the fundamental period of the signal, and the pressure inside the cavity can be captured by a linear theory. For small membrane deformation ($\varepsilon < 0.5$), the membrane opens until a hole of about $l_c \simeq 2$ mm diameter, which remains stable in time. Due to this partial opening, and the fact that $l_c \ll \Phi$, the diameter of the cavity, the system acts as a resonator with symmetric boundary conditions, which has a direct influence on the acoustic signal frequency content. Finally, for intermediate membrane tension ($0.5 \leq \varepsilon \leq 2$), the rupture occurs in two steps: an initial step where the opening progresses slowly; after reaching a critical size, the fracture then propagates quickly, until the membrane is fully opened.

A transversal wave is excited along the membrane surface, and is clearly visible in both the stable hole and the two-step opening dynamics. We have shown that it can be interpreted in the framework of fracture propagation in a brittle material. The characteristic fracture velocity, v_s , corresponds to the transverse wave velocity. Despite the inherent dispersion of data, this theory makes it possible to infer the experimental dependence of the rupture time on the membrane initial strain, $\tau_{\text{rup}} = a/\sqrt{\varepsilon}$, for the two-step opening regime.

The wave propagating on the membrane has a direct signature on the acoustic signal. We report that this additional acoustic signal gets stronger when the rupture time increases (see fig. 4). A thorough study of the link between the characteristics of this additional wave and the properties of the membrane (elastic response, initial strain, etc.) is out of the scope of this paper. However, it is interesting to point out that in field situations such as on volcanoes, this relationship could represent an indirect way to estimate the rupture time, *i.e.* the initial tension stored on the giant bubble cap exploding at the surface of the volcanic conduit. This could provide more information both on magma properties and on the bubble overpressure or decompression rate.

The authors acknowledge one anonymous referee and Dr. A. Namiki for greatly improving the manuscript. In particular, we thank A. Namiki for providing a possible mechanism to explain why the pressure decay time is slightly larger than the membrane rupture time. This work was supported by the international project ECOS Sud-CONICYT #C14E07 and by the LABEX iMUST (ANR-10-LABX-0064) of Université de Lyon, within the program "Investissements d'Avenir" (ANR-11-IDEX-0007) operated by the French National Research Agency (ANR). CS is grateful to CONICYT scholarship Doctorado-2011 for financial support CONICYT 21110609.

References

1. D.E. Speil, J. Geophys. Res. **97**, 11443 (1992).
2. G.B. Deane, J. Acoust. Soc. Am. **133**, 69 (2013).
3. D.T. Deihl, F.R. Carlson, Am. J. Phys. **36**, 441 (1968).

4. J. Lighthill, *Waves in Fluids* (Cambridge University Press, Cambridge, UK, 1978) p. 504.
5. M.R. James, S.J. Lane, B. Chouet, J.S. Gilbert, J. *Volcanol. Geotherm. Res.* **129**, 61 (2004).
6. R.B. Bird, R.C. Armstrong, O. Hassager, *Dynamics of Polymeric Liquids*, Vols. **I** and **II** (Wiley, New York, 1987).
7. R.P. Chhabra, *Bubbles, Drops and Particles in non-Newtonian Fluids*, 2nd edition, Chemical Industries (Taylor & Francis, London, 2007) Series No. 113.
8. T. Kobayashi, A. Namiki, I. Sumita, J. *Geophys. Res.* **115**, B10201 (2010).
9. V. Vidal, J.-C. Géminard, T. Divoux, F. Melo, *Eur. Phys. J. B* **54**, 321 (2006).
10. T. Divoux, V. Vidal, F. Melo, J.-C. Géminard, *Phys. Rev. E* **77**, 056310 (2008).
11. V. Vidal, M. Ripepe, T. Divoux, D. Legrand, J.-C. Géminard, F. Melo, *Geophys. Res. Lett.* **37**, L07302 (2010).
12. C. Sánchez, B. Álvarez, F. Melo, V. Vidal, *Geophys. Res. Lett.* **41**, 6705 (2014).
13. A. Yokoo, M. Iguchi, J. *Volcanol. Geotherm. Res.* **196**, 287 (2010).
14. J.B. Johnson, M. Ripepe, J. *Volcanol. Geotherm. Res.* **206**, 61 (2011).
15. E. Blackburn, L. Wilson, R. Sparks, *J. Geol. Soc. London* **132**, 429 (1976).
16. S. Vergnolle, G. Brandeis, *J. Geophys. Res.* **101**, 20433 (1996).
17. M. Hagerty, S. Schwartz, M. Garcés, M. Protti, J. *Volcanol. Geotherm. Res.* **101**, 27 (2000).
18. S. Vergnolle, M. Boichu, J. Caplan-Auerbach, J. *Volcanol. Geotherm. Res.* **137**, 109 (2004).
19. H.M. Gonnermann, M. Manga, *Annu. Rev. Fluid Mech.* **39**, 321 (2007).
20. J. Taddeucci, M.A. Alatorre-Ibargüengoitia, M. Moroni, L. Tornetta, A. Capponi, P. Scarlato, D.B. Dingwell, D. De Rita, *Geophys. Res. Lett.* **39**, L16306 (2012).
21. L. Mullins, *Rubber Chem. Technol.* **42**, 339 (1947).
22. J. Diani, B. Fayolle, P. Gilormini, *Eur. Polym. J.* **45**, 601 (2009).
23. J. Niemczura, K. Ravi-Chandar, *J. Mech. Phys. Solids* **59**, 457 (2011).
24. H. Levine, J. Schwinger, *Phys. Rev. Lett.* **73**, 383 (1948).
25. L.E. Kinsler, A.R. Frey, A.B. Coppens, J.V. Sanders, *Fundamentals of Acoustics*, 3rd edition (J. Wiley & Sons, Inc., New York, 1982).
26. A. Pierce, *Acoustics - An Introduction to Its Physical Principles and Applications* (ASA, New York, 1989).
27. J. Kemp, *Theoretical and experimental study of wave propagation in brass musical instruments* PhD thesis, University of Edinburgh (2002).
28. R. Vermorel, N. Vandenberghe, E. Villermaux, *Proc. R. Soc. A* **463**, 641 (2006).
29. P. Oswald, *Rhéophysique, Ou comment coule la matière* (Belin, Collection Echelles, 2005).